Romanian Reports in Physics, Vol. 68, No. 2, P. 630–641, 2016

SPECTROSCOPIC AND COMPUTATIONAL INVESTIGATION OF A THIAZOLIDINE -2, 4-DIONE COMPOUND

I.B. COZAR[1*], A. PÎRNĂU[1], L. SZABO[2], N. VEDEANU[3], C. NASTASĂ[3]

[1] National Institute for Research and Development of Isotopic and Molecular Technologies, RO-400293 Cluj-Napoca, Romania
[2] "Babes-Bolyai" University, Faculty of Physics, 1 Kogalniceanu, 400084 Cluj-Napoca, Romania
[3] "Iuliu Hatieganu" University of Medicine and Pharmacy, Faculty of Pharmacy, RO-400023 Cluj-Napoca, Romania
[*] Corresponding author: bogdan.cozar@itim-cj.ro

Received December 9, 2014

Abstract. Bacterial resistance has become a serious public health problem, demanding the new compounds, with structures and targets of action, able to deal with resistant bacteria. In this context the potential antimicrobial 3-[2-(4-Methyl-2-phenyl-thiazol-5-yl)-2-oxo-ethyl]-thiazolidine-2,4-dione compound was synthesized and investigated by FT-IR, FT-Raman, ^{1}H, ^{13}C NMR spectroscopies and also by DFT calculations at B3LYP/6-31G(d) level of theory. The very good correlation found between the experimental and theoretical data shows that the optimized molecular structure is very close to reality. Also the NMR spectra show a monomeric behaviour of this compound in solutions.

Keywords: Thiazolidine compound, IR, Raman, NMR, DFT.

1. INTRODUCTION

The treatment of infectious diseases is an important and challenging problem due to a combination of factors, including emerging infectious diseases and the increasing number of multi-drug resistant microbial pathogens. Bacterial resistance has become a serious public health problem, demanding new classes of antibacterial agents [1, 2]. A potential approach to overcome the resistence problem may be represented by the design of innovative agents having a different mechanism of action, without any cross-resistence with the therapeutic agents already in use. Thiazoles and their derivatives have attracted the interest over the last decades because of their varied biological activities: antifungal, anti-inflammatory, anti-allergic [3–6].

In this context, new thiazolidinedione compounds (TZDs) as potential anti-inflamatory agents in an acute experimental inflammation were synthesized and also investigated for their antimicrobial properties [7].

The 3- [2- (4- methyl- 2-phenyl - thiazol-5-yl)-2 -oxo-ethyl]-thiazolidine-2,4-dione compound was obtained in 3 steps according to Scheme 1 [8, 9].

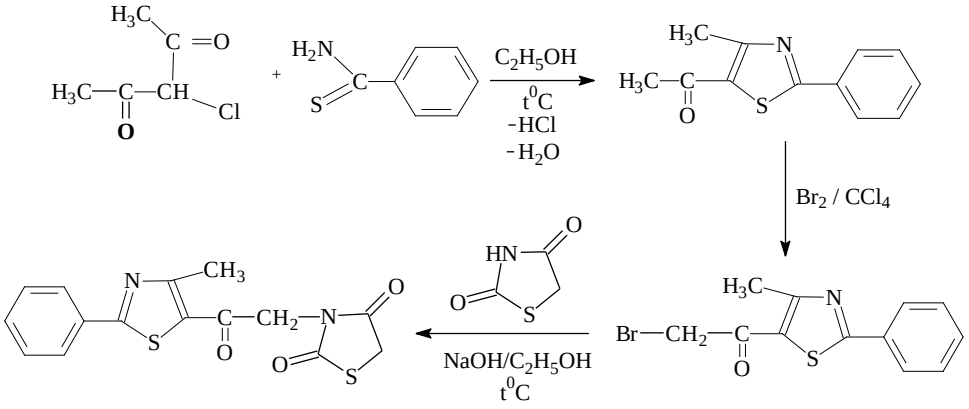

Scheme 1.

First of all 5-bromoacetyl-4-methyl-2-phenyl-thiazol was obtained by refluxing thiobenzamide with α-chlor-acetylacetone, in absolute ethanol. This compound was then transformed in a bromo derivate [8], that finally reacted with thiazolidine-2,4-dione in ethanol, in the presence of sodium hydroxide conforming with literature data [9].

Structural investigations on compounds of biomedical and pharmacological interest are increasingly reported in the last years in the scientific literature. For this goal, experimental methods like FTIR, Raman, SERS, NMR and quantum chemical calculations based on density functional theory (DFT) were successful used in order to a good understanding of their pharmacological activity [10–15].

To the best of our knowledge, assignment of the normal vibrational modes of this compound on IR and Raman spectroscopies coupled with quantum chemical calculations has not been done so far.

For a proper understanding of the IR and Raman spectra and a reliable assignment of all vibrational bands, DFT calculations, particularly those based on hybrid functional methods [16] have evolved to a powerful quantum chemical tool for the determination of the electronic structure of molecules. In this framework, the B3LYP hybrid exchange-correlation functional is one of the most used since it proved its ability in reproducing various molecular properties, including vibrational spectra. The combined use of B3LYP functional and standard split valence basis set 6-31G(d) has been previously shown [17, 18] to provide an excellent

compromise between accuracy and computational efficiency of vibrational spectra for large and medium-size molecules.

Thus, the structural investigations by vibrational spectroscopic methods (FTIR, Raman) and ^{1}H, ^{13}C NMR, as well as density functional theory (DFT) based calculations performed on TZD molecule are reported in this paper.

2. EXPERIMENTAL

FT-IR and FT-Raman spectra of TZD powder were recorded at room temperature on a conventional Equinox 55 (Bruker Optik HmbH, Ettlinger, Germany) FT-IR spectrometer, equipped with an InGaAs detector, coupled with a Miracle (PIKE Technologies) ATR sampling device with a single reflection ZnSe crystal plate as the internal reflection element. Before recording the FT-IR/ATR spectrum a background spectrum was recorded in order to eliminate the absorptions of atmospheric water and carbon dioxide. A standard ATR intensity correction performed by the OPUS software was applied.

The FT-Raman spectrum of TZD was recorded in backscattering geometry with a Bruker FRA 106/S Raman accessory equipped with a nitrogen cooled Ge detector. The 1064 nmNd:YAG laser was used as excitation source, and the laser power measured at the sample was 300 nW. The FT-IR, FTIR/ATR and FT-Raman spectra were recorded with a resolution of 4 cm^{-1} by co-adding 32 scans.

The ^{1}H and ^{13}C NMR spectra of this new compound were recorded at room temperature on a Bruker Avance III NMR spectrometer operating at 500 MHz for ^{1}H and 125.76 MHz for ^{13}C, internal standard TMS. The samples were prepared by dissolving this new compound in DMSO-d_6 (signal for ^{1}H at 2.512 ppm and at 39.95 ppm for ^{13}C). The spectra were recorded using a single excitation pulse of 10.1 μs for ^{1}H and 8 μs for ^{13}C. The FID signal was acquired 32 times for ^{1}H and 1024 times for ^{13}C.

3. RESULTS AND DISCUSSION

3.1. IR SPECTRA

The B3LYP/6-31G(d) optimized geometry of studied compound is given in Fig. 1.

Experimental and calculated FT – IR spectra in the 400–3200 cm^{-1} region are shown in Fig. 2.

Representative experimental FT-IR bands together with calculated wavenumbers and their assignments are given in Table 1.

The bands from 509 cm^{-1} and 657 cm^{-1} are due to the in plane deformations and breathing vibrations of ring 3, respectively. Also the band at 685 cm^{-1} is characteristic of the in plane deformations of rings 1 and 2. The band from 795cm^{-1} is due to the out of plane bending vibrations characteristics of ring 1 CH groups.

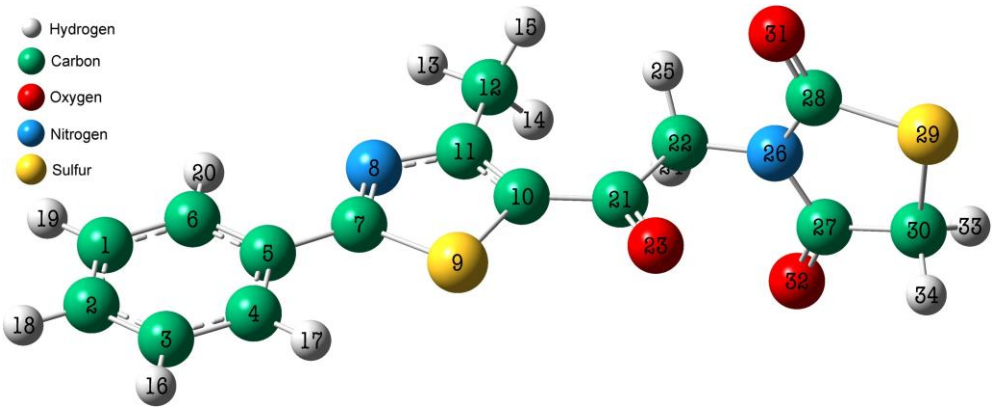

Fig. 1 – The B3LYP/6-31G(d) optimized geometry
of 3-[2-(4-Methyl-2-phenyl-thiazol-5-yl)-2-oxo-ethyl]-thazolidine-2,4-dione.

A superposition between breathing vibrations of ring 1 and ring 2 with deformation vibrations of C22-H_2 group appears at 964 cm^{-1}. Other superpositions between rocking and bending vibrations of C22-H_2 group and asymmetric stretching vibration of C28-N267-C27 group are evidenced at 1003 cm^{-1} and 1138 cm^{-1}, respectively.

The band which appears at 1234 cm^{-1} in the FT-IR spectrum is due to the superposition of C5-C7, C21-C10, C11-N8 bonds stretching vibrations with bending vibrations of C22-H_2 group and ring 1 CH groups.

The bands from 1352 cm^{-1} and 1378 cm^{-1} are due to the superpositions of C22-N26, C27-N26 stretching vibrations with C22-H_2 group bending vibration and bending C22-H_3 group vibrations with stretching C11-C12 vibration, respectively.

Another complex superposition between stretching vibrations of C7=N8, C5-C7, C1-C12 bonds with bending vibrations of C12-H_3 group is evidenced at 1417 cm^{-1}.

The intens band from 1669 cm^{-1} is due to the superposition of stretching C21=O vibration with bending vibration of C22-H_2 group.

The last band from 1747 cm^{-1} is assigned to asymmetric stretching vibration of C27=O and C28=O groups.

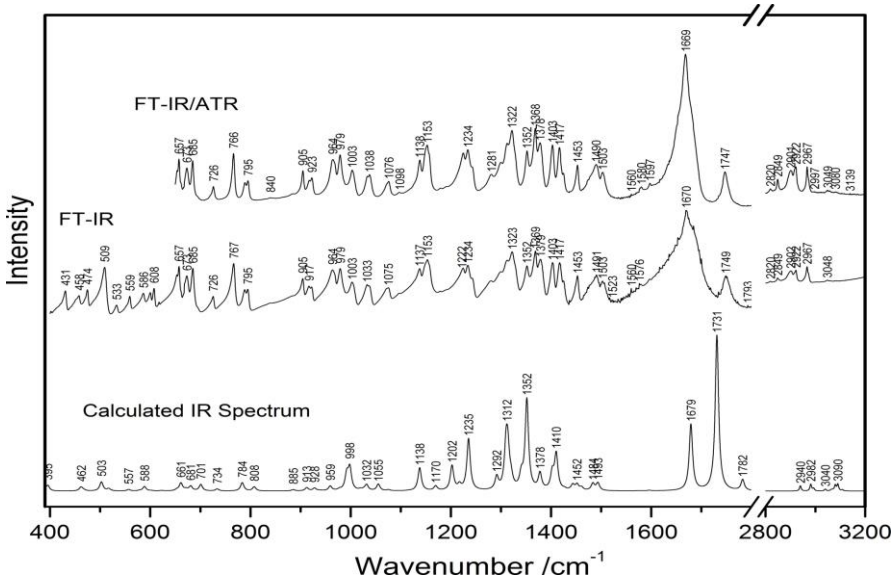

Fig. 2 – Experimental FTIR and calculated IR spectra of TZD compound.

Table 1

Selected experimental FT-IR bands together with calculated wavenumbers and their assignments

Experimental wavenumbers (cm^{-1})		**Calculated wavenumbers (cm^{-1})***	
FTIR/ATR	**FTIR**	**B3LYP**	**Band assignment****
	509	503	ip. ring3 deformation
657	657	661	ring3 breathing
685	685	681	ip. ring1, ring2 deformation
795	795	784	δ_{op}(ring1 CH)
964	964	959	ring1 breathing, δ(C22-H_2), ring2 breathing, ν(C21-C22)
1003	1003	998	ρ(C22-H_2), ν_{as}(C28-N26-C27)
1138	1137	1138	δ(C22-H_2), ν_{as}(C28-N26-C27)
1234	1234	1235	ν(C5-C7, C21-C10, C11-N8), δ(C22-H_2), δ(ring1 CH)
1322	1323	1312	δ(ring1 CH), δ(C22-H_2), δ(C12-H_3), ν(C7═N8)
1352	1352	1352	ν(C22-N27, C27-N26, C22-N27), δ(C22-H_2)
1378	1379	1378	δ(C12-H_3), ν(C11-C12)
1417	1417	1410	ν(C7═N8, C5-C7, C11-C12), δ(C12-H_3)
1669	1670	1679	ν(C21═O), δ(C22–H_2)
1747	1749	1731	ν_{as}(C27═O, C28═O)

* – scaled values according to Scott and Radom [19].
** – ν – stretching, ν_{as} – asymmetric stretching, ν_s – symmetric stretching, δ-in-plane bending, ρ – rocking, op. – out of plane, ip. – in plane; ring 1 – benzene (C1-C6), ring 2 – (C7-S9-C10-C11-N8), ring 3 – (N26-C27-C30-S29-C28).

3.2. RAMAN SPECTRA

Experimental and calculated Raman spectra of the investigated molecule are shown in Fig. 3. The most intense Raman bands, experimental and calculated, together with their assignments are given in Table 2.

The in plane deformations of ring 1 and ring 2 superimposed with bending vibrations of $C12H_3$ group appear at 605 cm^{-1}.

Another overlap of the in plane deformations and breathing vibrations of ring 1 with bending vibrations of $C12H_3$ group is situated at 1002 cm^{-1}.

The band from 1177 cm^{-1} is due to the bending vibrations of benzene (ring 1) CH groups.

A superposition between breathing vibrations of ring 1 and ring 2 with stretching vibrations of C21-C10, C7-C5, S9-C10 bonds and bending vibration of $C22H_2$ group appears at 1280 cm^{-1}.

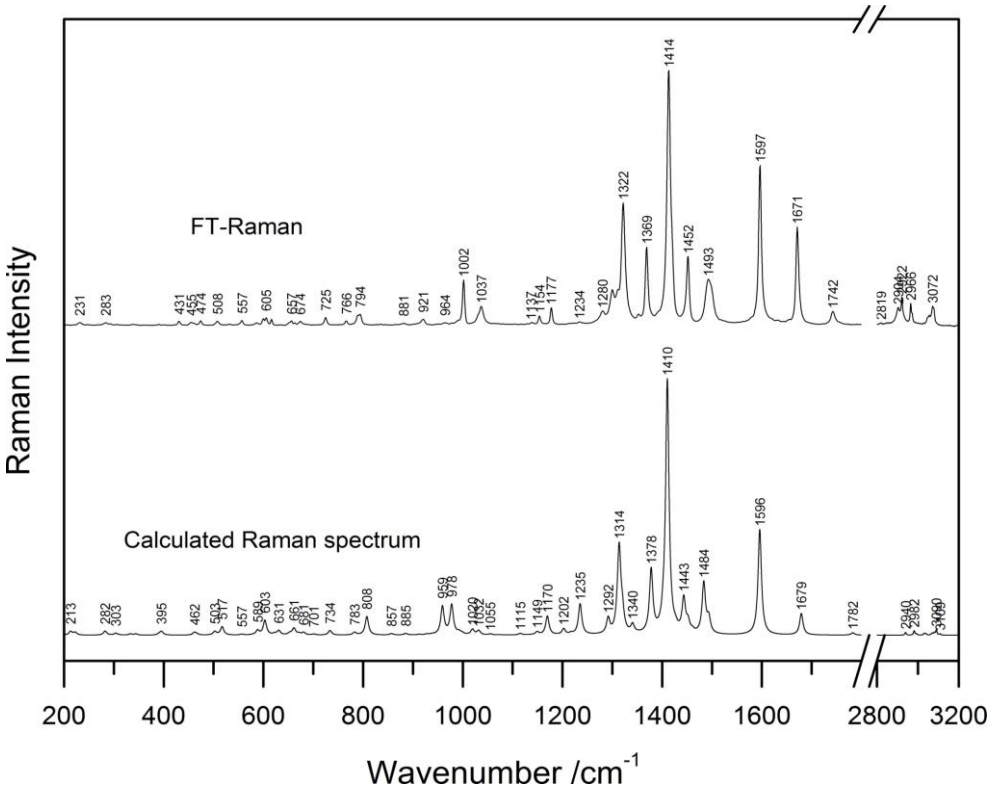

Fig. 3 – Experimental FT-Raman and calculated Raman spectra of TZD compound.

Table 2

Selected experimental FT-Raman bands together with calculated wavenumbers and their assignments

Experimental wavenumbers (cm^{-1})	**Calculated wavenumbers (cm^{-1})***	
FT-Raman	**B3LYP**	**Band assignment****
605	603	ip. ring2 ring3 deformation, $\delta(C12H_3)$
1002	978	ring1 breathing, ip. ring1 deformation, $\delta(C12H_3)$
1177	1170	δ(ring1 CH)
1280	1292	ring2 ring1 breathing, ν(C21-C10, C7-C5), ν(S9-C_2), $\delta(C22H_2)$, δ(ring1 CH), ν(CC ring1)
1322	1314	ν(N8-C1), δ(ring1 CH), $\delta(C12H_3)$
1369	1378	$\delta(C12H_3)$, $\delta(C22H_2)$
1414	1410	ring2 breathing, ν(C11-C12, C11-C10, C7-C5), $\delta(C12H_3)$, δ(ring1 CH), ν(CC ring1)
1452	1443	ν(C11-C10), $\delta(C12H_3)$, δ(ring1 CH), ν(CC ring1)
1493	1484	ν(C11-C10), $\delta(C12H_3)$, δ(ring1 CH), ν(CC ring1)
1597	1596	ν(CC ring1), δ(CH ring1)
1671	1679	ν(C21═O), $\delta(C22\text{-}H_2)$

* – scaled values according to Scott and Radom [19].
** – ν – stretching, ν_{as} – asymmetric stretching, ν_s – symmetric stretching, δ-in-plane bending, op. – out of plane, ip. – in plane; ring 1– benzene (C1-C6), ring 2 – (C7-N8-C11-C10-S9), ring 3 – (N26-C27-C30-S29-C28).

The two intens bands from 1322 cm^{-1} and 1369 cm^{-1} are assigned to the superposition of stretching ν(N8-C11) vibration with bending vibrations of $C12H_3$, ring 1 CH groups and those between $C12H_3$, $C22H_2$ groups bending vibrations, respectively.

The most intens band situated at 1414 cm^{-1} is due to the superposition of breathing vibrations of ring 2 with stretching vibrations of C11-C12, C11-C10, C7-C5 bonds and $C12H_3$ group bending vibrations.

Both two bands from 1452 cm^{-1} and 1493 cm^{-1} are due according to calculations to the superpositions of stretching C11-C10 and bending vibrations of $C12H_3$ and ring 1 CH groups. An other superposition of stretching CC vibrations (ring 1) with bending vibrations of ring 1 CH groups gives rise to the intense band at 1597 cm^{-1}.

Stretching vibrations of double bond C21=O23 and bending vibrations of $C22\text{-}H_2$ group appear in the experimental Raman spectrum at 1671 cm^{-1}.

The very good correlation found between the experimental and theoretical data shows that the optimized structure is very close to reality.

3.3. MOLECULAR ELECTROSTATIC POTENTIAL (MEP)

Molecular electrostatic potentials have been used extensively for interpreting and predicting the reactive behavior of a wide variety of chemical systems in both

electrophilic and nucleophilic reactions, the study of biological recognition processes and hydrogen bonding interactions [14, 18].

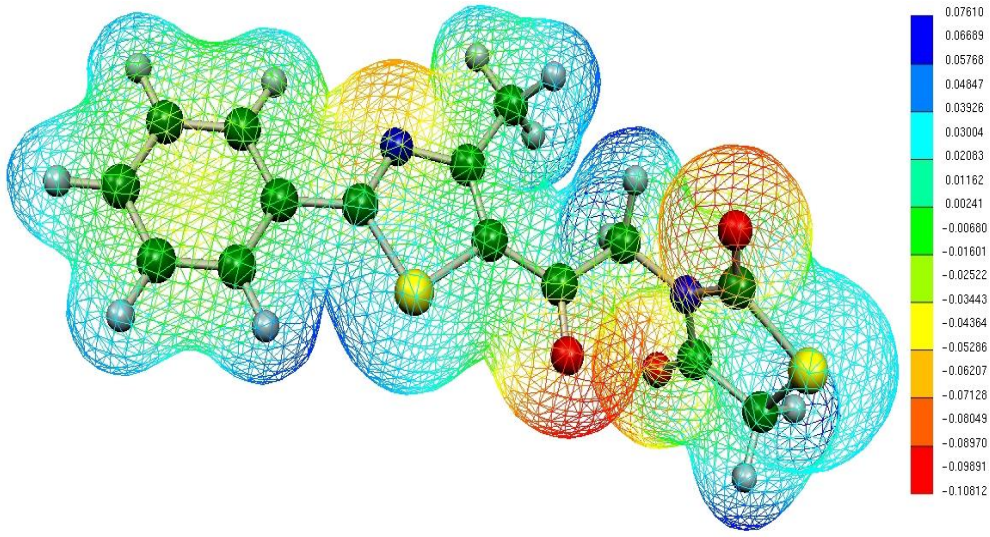

Fig. 4 – B3LYP/6-31G(d) calculated 3D electrostatic potential contour map of the studied molecule (a.u.).

To predict reactive sites for electrophilic and nucleophilic attack for the investigated compound, molecular electrostatic potential (MEP) was calculated at the B3LYP/6-31G(d) optimized geometries.

Figure 4 shows the calculated surface mapped 3D electrostatic potential in [a.u.], the electron density isosurface being 0.02 a.u.

The negative regions are related to electrophilic reactivity and the positive ones to nucleophilic reactivity. As can be seen in Fig. 1b this molecule has several negative regions associated with O23, O31 and O32 atoms. The most negative value of –0.1081 a.u. is associated with O23 atom while the values for O31 and O32 are about –0.0897 a.u., and –0.08049 a.u., respectively. Thus, it would be predicted that an electrophile will preferentially attack this molecule at the O23 position and then the positions O31, O32.

Alternatively, we found a maximum value of 0.04847 a.u. on the CH_2 and CH_3 groups region indicating that these sites can be the most probably involved in nucleophilic processes.

The MEP of this molecule suggests also an inclined adsorbed orientation on the silver nanoparticles by the oxygen atoms.

3.4. NMR SPECTRA

The ^{1}H and ^{13}C NMR measurements on the investigated compound were made on liquid state samples, using DMSO-d_6 as deuterated solvent (gives a residual peak of water at about 3.37 ppm [20] in ^{1}H NMR spectrum) and the corresponding experimental ^{1}H NMR spectrum is given in Fig. 5a. The aromatic protons (ring 1) give signals in 7–8 ppm range, the two methylene groups give signals to 4.95 and 4.42 ppm, respectively and the protons of the methyl group appear at 2.76 ppm. The values of peak integrals nicely reproduce the number of protons from each group.

From the ^{13}C NMR spectrum (Fig. 5b) we can observe the signal of ^{13}C from DMSO-d_6 solvent at 39.95 ppm, the ^{13}C signal of the methyl group C12 at 19.02 ppm and ^{13}C signals of the methylene groups C30 and C22 at 34.55 ppm and 49.65 ppm, respectively. Some equivalent ^{13}C signals of the aromatic ring appear in the same place in the spectrum as equivalent carbons: C1 and C3 at 127.27 ppm, C4 and C6 at 129.97 ppm, C2 at 128.82 ppm. The signals for the quaternary carbon atoms C5 and C10 appear at 132.39 ppm and 132.31 ppm, respectively, for C11 at 160.84 ppm, C7 at 170.57 ppm, C27 at 171.97 ppm, C28 at 172.32 ppm and C21 at 185.11 ppm.

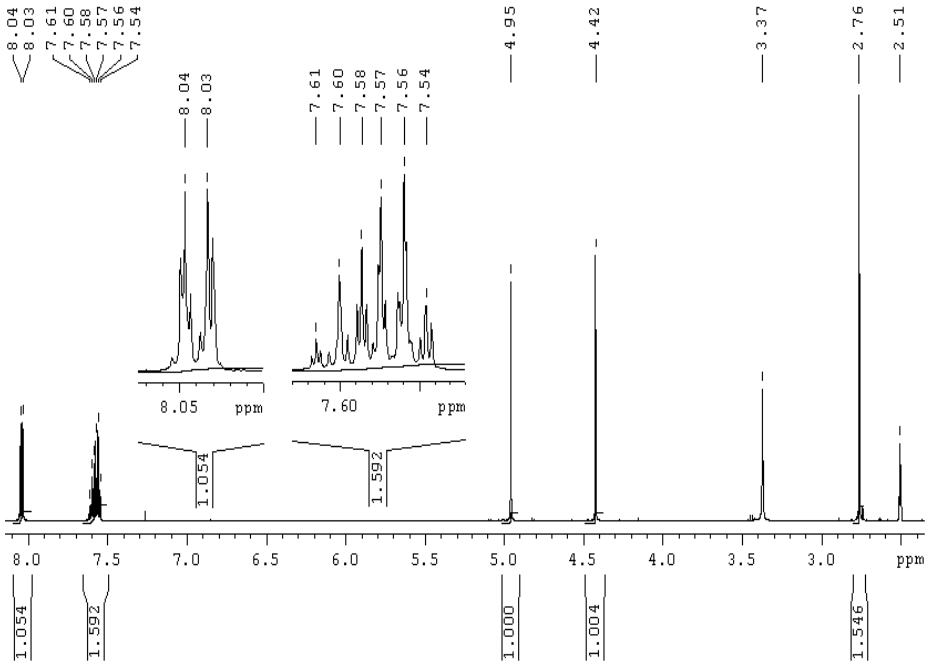

(a)

Fig. 5

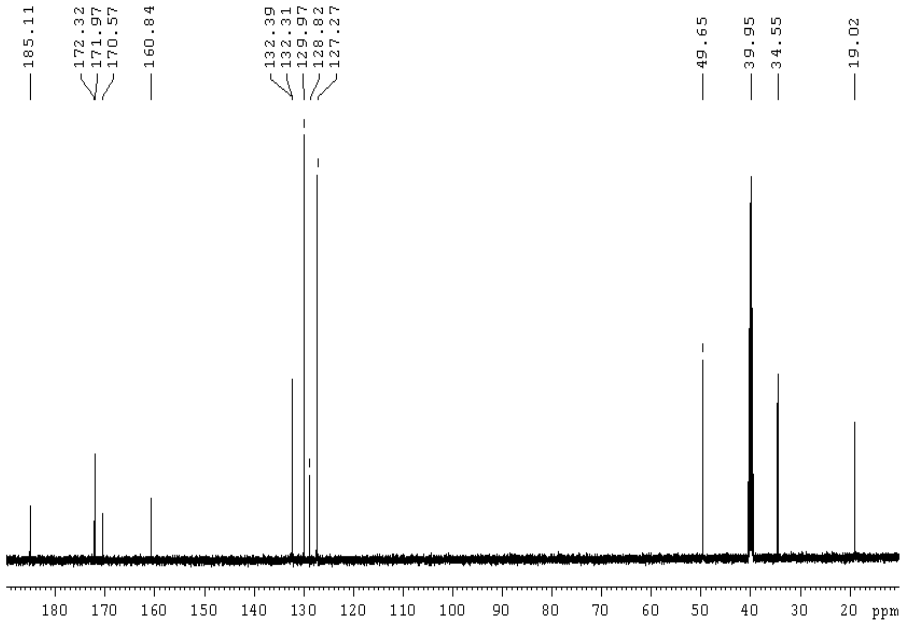

(b)

Fig. 5 (continued) – ^{1}H NMR (a) and ^{13}C NMR (b) experimental spectra of TZD compound in DMSO solution.

All NMR chemical shifts for ^{1}H and ^{13}C nuclei are given in Table 3.

Table 3

^{1}H and ^{13}C experimental chemical shifts of TZD (ppm)

^{1}H				^{13}C			
H17	8.04	H33	4.42	C21	185.11	C4	129.97
H20	8.04	H34	4.42	C28	172.32	C6	129.97
H16	7.57	H13	2.76	C27	171.97	C2	128.82
H18	7.57	H14	2.76	C7	170.57	C1	127.27
H19	7.57	H15	2.76	C11	160.84	C3	127.27
H24	4.95			C5	132.39	C22	49.65
H25	4.95			C10	132.31	C30	34.55
						C12	19.02

Due to the fact that the shape of both ^{1}H and ^{13}C NMR spectra, the number of resonance peaks and their associated chemical shifts are in agreement with the proposed structure, result that NMR data according with those vibrationals confirm the optimized structure of TZD (Fig. 1). As is shown in paper [14] the appearance of solute – DMSO complex leads to a chemical shift for hydrogen-bonded proton of about 14 ppm. Because in the ^{1}H NMR spectrum of the studied compound no

signal appears at a great ppm value (>10 ppm) or other significant shifts, it may be concluded the absence of any dimeric species (solute – solute, solute – solvent molecule) for the investigated compound.

4. CONCLUSIONS

Vibrational FT-IR, FT-Raman and NMR spectroscopies and also DFT calculations were successfully used to obtain the structural details on a new potential antimicrobial TZD compound.

All the representative experimental vibrational bands were assigned in agreement with theoretical calculations at B3LYP/6-31G(d) level of theory.

The very good correlation between experimental and theoretical data suggests that the optimized molecular structure is very close to reality.

The calculated surface mapped 3D electrostatic potential predict the electrophilic and nucleophilic reactive attack sites for the investigated molecule and also its possible orientation adsorbed on the silver nanoparticles.

Also the NMR spectra show a monomeric behaviour of this compound in solutions.

Acknowlegements. This work was supported by grants of the Romanian National Authority for Scientific Research, CNCS-UEFISCU, project number PN-II-ID-PCCE-2011-2-0027(BIOSENS) and PN-II-RU-TE-2012-3-0227.

REFERENCES

1. C. Franchini, M. Muraglia, F. Corbo, M. A. Florio, A. Di Mola, A. Rosato, R. Matucci, M. Nesi, F. van Bambeke, C. Vitali, Arch. Pharm. Chem. Life Sci. **342**, 605 (2009).
2. Y. Özkay, Y. Tunali, H. Karaca, I. Işikdağ, Arch. Pharm. Chem. Life Sci. **11**, 264 (2011).
3. H. S. Sader, D. M. Johnson, R. N. Jones, Antimicrob. Agents and Chemother. **48**, *1*, 53 2004.
4. M. Kurazono, I. Takashi, K. Yamada, Y. Hirai, T. Maruyama, E. Shitara, M. Yonezawa, Antimicrob. Agents and Chemother. **48**, *8*, 2831 (2004).
5. A. De Logu, M. Saddi, M. C. Cardia, R. Borgna, C. Sanna, B. Saddi, E. Maccioni, J. Antimicrob. Chemother. **55**, 692 (2005).
6. C.M. Moldovan, O.Oniga, A. Pârvu, B. Tiperciuc, Ph. Verite, A. Pîrnău, O. Crişan, M. Bojiţă, R. Pop, Eur. J. Med. Chem. **46**, 526 (2011).
7. C. Nastasă, B. Tiperciuc, A. Pârvu, M. Duma, I. Ionuţ, O.Oniga, Arch. Pharm. Chem. Life Sci. **346**, 481 (2013).
8. L. Costea, O. Oniga, M. Ionescu, B. Tiperciuc, D. Ghiran, Farmacia **53**, *2*, 67 (2005).
9. O. Bozdag-Dundar, O.Ozgen, A. Mentese, N. Altanlar, O. Atli, E. Kendi, R. Ertan, Bioorg. and Med. Chem. **15**, 6012 (2007).
10. M. Baia, S. Astilean, T. Iliescu, Raman and SERS Investigations of Pharmaceuticals, Springer-Verlag, Berlin, 2008.
11. N. Leopold, Surface Enhanced Raman Spectroscopy – Selected Applications, Edit. Napoca Star, Romania, 2009.

12. N. Beckmann, R. Kneuer, H.U. Gremlich, H. Karmouty-Quintana, F.X. Blé, M. Müller, NMR in Biomedicine **20**, 154 (2007).
13. L. Szabó, V. Chiş, A. Pîrnău, N. Leopold, O. Cozar, Sz. Orosz, J. Mol. Struct. **924–926**, 385 (2009).
14. A. Pîrnău, V. Chiş, L. Szabo, O. Cozar, M. Vasilescu, O. Oniga, R.A. Varga, J. Molec. Struct. **924–926**, 361 (2009).
15. A. Pîrnău, M. Bogdan, M. Mic, M. Palage, R.A. Varga, Rom. Journ. Phys. **59**, 550 (2014).
16. R.G. Parr, W. Yang, Density-functional Theory of Atoms and Molecules, Oxford University Press, New York, 1989.
17. I.B. Cozar, L. Szabo, N. Leopold, V. Chiş, O. Cozar, L. David, J. Molec. Struct. **993**, 308 (2011).
18. L. Szabo, K. Herman, N.E. Mircescu, A. Fălămaş, L.F. Leopold, N. Leopold, C. Buzumurgă, V. Chiş, Spectrochim. Acta **A93**, 266 (2012).
19. A.P. Scott, L. Radom, J.Phys. Chem. **100**, 16502 (1996).
20. H.E. Gottlieb, V. Kotlyar, A. Nudelman, J. Org. Chem. **62**, 7512 (1997).